Spatio-Temporal Analysis of Climate Change Parameters Using Satellite Data for the Southeast Asian Region

S. C. Liew*, A. S. Chia, L. K. Kwoh

Centre for Remote Imaging, Sensing and Processing, National University of Singapore
10 Lower Kent Ridge Road, Blk S17 level 2, Singapore 119076
(scliew, crscas, lkkwoh)@nus.edu.sg

Abstract – The spatial and temporal variations of several environmental parameters over the Southeast Asia region recorded by remote sensing satellites for the past one to two decades are examined in relation to climate change. At the South China Sea, an increasing trend for sea surface temperature at a rate of 0.1 to 0.5 degree per decade was observed while the sea level anomaly increases at 2 to 6 cm per decade. The vegetation index of Kalimantan shows strong seasonal variations and a significantly decreasing trend. Several areas with increasing aerosol optical thickness were observed where land clearing and biomass burning activities were common. Precipitation rate and sea level anomaly show dominant association with annual seasonal monsoons and moderate association with El-Nino influences. The precipitation rate does not seem to have significant correlation with the global warming index.

Keywords: Climate change, spatio-temporal analysis, regression, empirical orthogonal function, satellite data.

1. INTRODUCTION

Earth observation satellites are useful in providing long term records of environmental parameters with global coverage. The records of satellite data exist since the seventies of the last century. Many good quality datasets are available which can be used in assessing trends in global climate and providing inputs to climate models. In this paper, we analyse the spatio-temporal trends of several environmental parameters over the Southeast Asian region using satellite data. The parameters studied are: sea surface temperature (SST), sea level anomaly (SLA), precipitation rate (PR), aerosol optical thickness (AOT) and normalized difference vegetation index (NDVI).

2. SATELITE DATA PRODUCTS

The source of the SST data is the AVHRR Pathfinder SST version 5.0 data set (Kilpatrick et al., 2001). The monthly averages of global 4-km SST data from 1985 to 2007 were acquired from NASA's Physical Oceanography Distributed Active Archive Center (PO.DAAC) and a subset covering the Southeast Asia region, including the South China Sea and eastern Indian Ocean was extracted for this study.

The sea level anomaly data set was obtained from the Data Unification Altimeter Combination System (DUACS) which is a part of SSALTO, the ground segment of the multi-mission altimetry program of the French space agency CNES. The primary satellites used in generating the SLA data are Topex/Poseidon and Jason-1 (Leuliette, 2004). Weekly mean SLA data generated by DUACS from 1992 to 2007 were acquired for this study.

The TRMM 3B43v6 monthly precipitation product is used in our analysis. This product was generated from the combined multisatellite sensors and calibrated with monthly rain gauge analysis from the Global Precipitation Climatology Project (GPCP) (Huffman et al., 2007).

The mean monthly AOT at wavelength of 550nm over land and ocean at 1 degree sampling grid points is used in this study. This monthly aggregated product is derived from the MOD04 aerosol product generated from each MODIS scene at 10 km resolution. This parameter is included in the MOD08_M3 monthly 1 degree global atmospheric product (King, 2003).

The MODIS monthly composite NDVI (MOD13C2) is used in this study. NDVI is a component in the MOD13 Vegetation Index product for MODIS. The NDVI values are calculated from the level 2 daily surface reflectance product (MOD09), to which atmospheric correction has already been applied. The monthly composite product (MOD13C2) is produced by temporal and spatial aggregates of cloud-free NDVI values onto a 0.05 deg x 0.05 deg equal-angle grid (Huete et al., 1999 and 2002).

3. METHODS

Linear regression was performed on the time series of each environmental parameter at each grid point over the area of study. The slope of the regression line gives an indication of rising or falling trend of the parameter concerned. The standard error of the slope was used to evaluate the statistical significance of the trend observed.

The empirical orthogonal function (EOF) analysis (Lorenz 1956, Bjornsseon and Venegas 1997) was used to investigate the spatial and temporal variations of an environmental parameter. Basically, the EOF analysis decomposes the spatio-temperal data into several modes of variations. Each mode can be associated with one or several mechanisms of variations. The EOF analysis is similar to the principal components analysis (PCA) commonly used for decorrelating a set of variables. The dataset of the observed parameter can be treated as a function $s(x, y, t)$ of the spatial coordinates (x, y) and time t. The EOF analysis basically decomposes $s(x, y, t)$ into a series of orthogonal functions $f_i(x, y)$ of the spatial coordinates only. The temporal variation is captured in a series of temporal functions $g(t)$ such that,

$$s(x, y, t) = \sum_{i=1}^{N} f_i(x, y) g_i(t) \qquad (1)$$

where N is the total number of observations made in time. The EOF's $f_i(x, y)$ and their respective coefficients $g(t)$ can be found by solving the eigenvalue equation constructed

from the covariance matrix of $s(x, y, t)$. The orthogonal functions $f_i(x, y)$ are arranged in decreasing order of the corresponding eigenvalues of the covariance matrix. Thus, the first few orthogonal functions usually account for most of the spatial variance that exists in the dataset.

4. RESULTS

4.1 Linear Regression Analysis

The mean daytime SST of the study area for the period from Jan 1985 to Sep 2007 is shown in Fig. 1. To illustrate the linear regression analysis, a point in the South China Sea (N6.50, E108.5) is examined. Fig. 2 shows the time series of the mean monthly SST at this point. The linear regression line has an increasing trend with a slope 0.13 ± 0.1 degC/decade. Fourier analysis reveals two dominant periods of 12 months and 6 months (Fig. 3). The climatology monthly SST are composed from the Fourier components (Fig. 3).
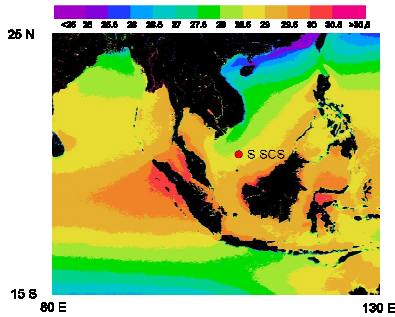
Fig. 1. Mean daytime SST for the period from Jan 1985 to Sep 2007.
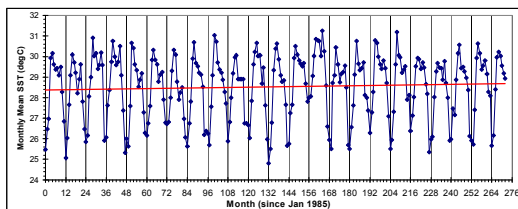
Fig. 2. Mean monthly daytime SST at a test point in the South China Sea. The red line is the linear regression line.
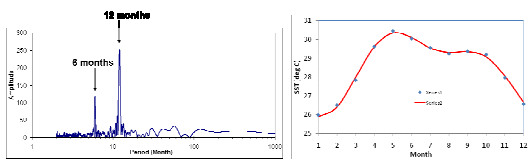
Fig. 3. Periodogram of the SST time series (left) and the climatology monthly SST composed from the Fourier components (right).
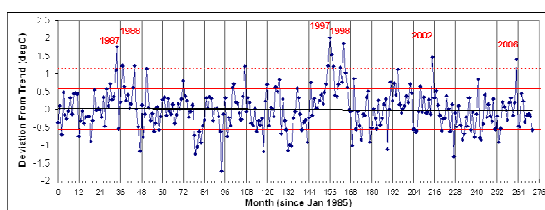
Fig. 4. Deviation of SST from the climatology + trend. Extreme values corresponding to El-Nino events are indicated.

The deviation of the monthly SST from the climatology + linear trend is shown in Fig. 4. The extreme events (2 standard deviations from the zero line) are seen to coincide with the El-Nino events of 1987-88, 1997-98, 2002 and 2006.
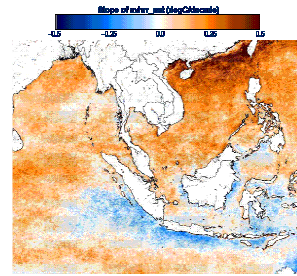
Fig. 5. Slope of linear regression of monthly mean SST.

Linear regression was performed at all grid points in the study area. The slope of the regression trend line is plotted in Fig. 5. The SST generally shows an increasing trend throughout the region, consistent with the observations of global warming. The magnitude is about 0.2 degC per decade but the rate can be as high as 0.5 degC per decade near the southern coast of China. However, the waters south of the Indonesia Archipelago exhibit a decreasing trend in SST.

Similar analysis was done for other parameters. Fig. 6 shows the slopes of regression for sea level anomaly (SLA), precipitation rate, aerosol optical thickness (AOT) and vegetation index (NDVI).
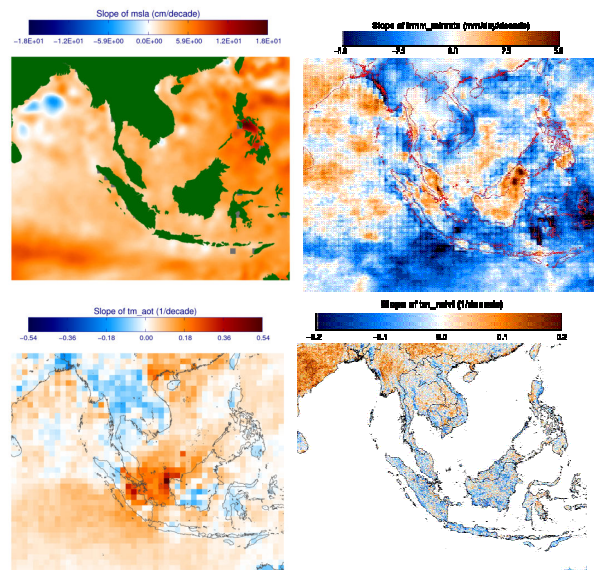
Fig. 6. Slope of linear regression of sea level anomaly (upper left), precipitation rate (upper right), aerosol optical thickness (lower left) and vegetation index (lower right).

The SLA shows an increasing trend throughout the region at a rate ranging from 2 to 6 cm per decade. The precipitation rate generally shows an increasing trend in Peninsular Malaysia, Borneo Island, the central part of Sumatra, and the Luzon and Mindanao islands of the Philippines. The increase in the precipitation rate is as high as 5 cm/day over the past decade. The Indochina regions of Myanmar, Lao PDR, Cambodia and south Vietnam show a decreasing trend in precipitation.

The mean AOT is generally low over the South China Sea and Indian Ocean (about 0.15 or less) and over land masses in the insular part of the region (around 0.2 to 0.3). However, in the southern coast of China, the mean AOT is higher (> 0.5). The AOT generally tends to be stable in time with the slope of linear regression close to zero. However, there are two patches of "hot spots" at the Riau Province and the northern part of West Kalimantan of Indonesia which show exceptionally high increasing trend of AOT with time.

The NDVI generally shows a neutral to decreasing trend. NDVI is associated with vegetation cover. The decrease in vegetation cover may be a manifestation of climate change but can also be due to anthropogenic activities.

4.2 EOF Analysis

EOF analysis is performed on the sea level anomaly data set. The first three modes are shown in Fig. 7. Mode 1 corresponds to the seasonal variation illustrated by the sinusoidal variations of the temporal coefficients. Mode 2 seems to be more erratic in its temporal pattern. However, its temporal coefficient is found to have a negative correlation with El-Nino with $R^2=0.49$ (Fig. 8 and Fig. 9).
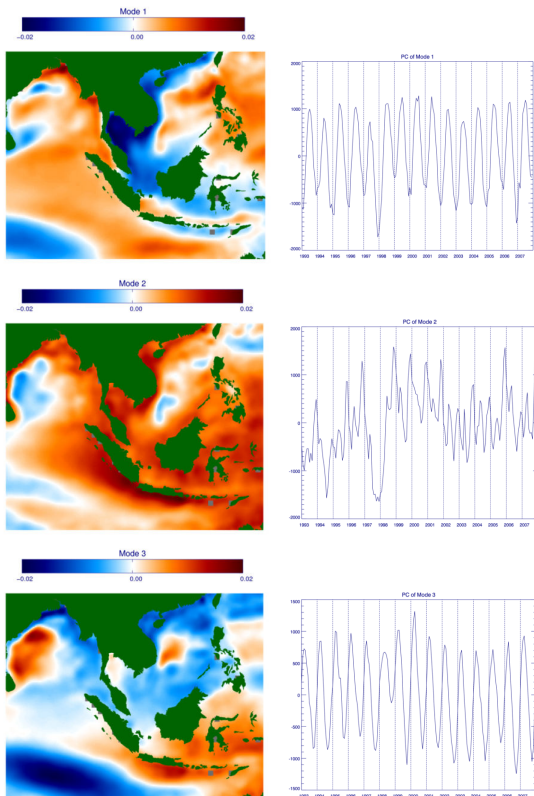
Fig. 7. The first three EOF modes of SLA (left column, from the top) EOF1, EOF2 and EOF3. The corresponding temporal coefficients are shown on the right column.

The first three modes of EOF analysis for the precipitation rate data set are shown in Fig. 10. Mode 1 corresponds to the seasonal variation of precipitation. This oscillation has a maximum in June-July and minimum in Dec-Jan. The spatial variation of this mode is illustrated in the corresponding EOF1. Positive values of EOF1 indicate the temporal variation in phase with the variations of the temporal coefficients while negative values indicate an out of phase variation.
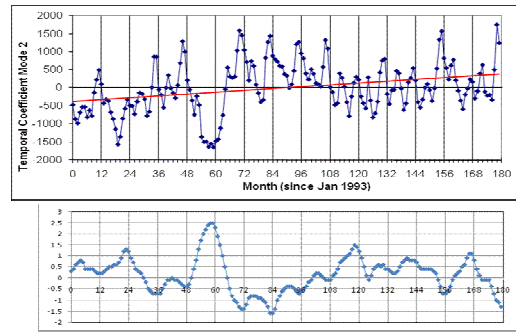
Fig. 8. EOF2 temporal coefficient of SLA (top) and monthly Ocean Nino Index (bottom) from Jan 1998 to Dec 2007.
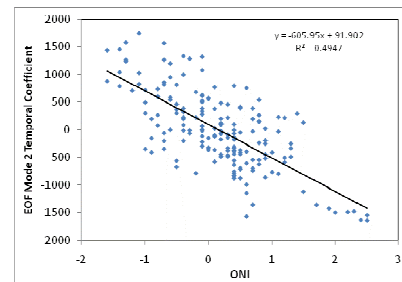
Fig. 9. Regression of SLA EOF mode 2 temporal coefficient with the Ocean Nino Index ($R^2 = 0.49$).
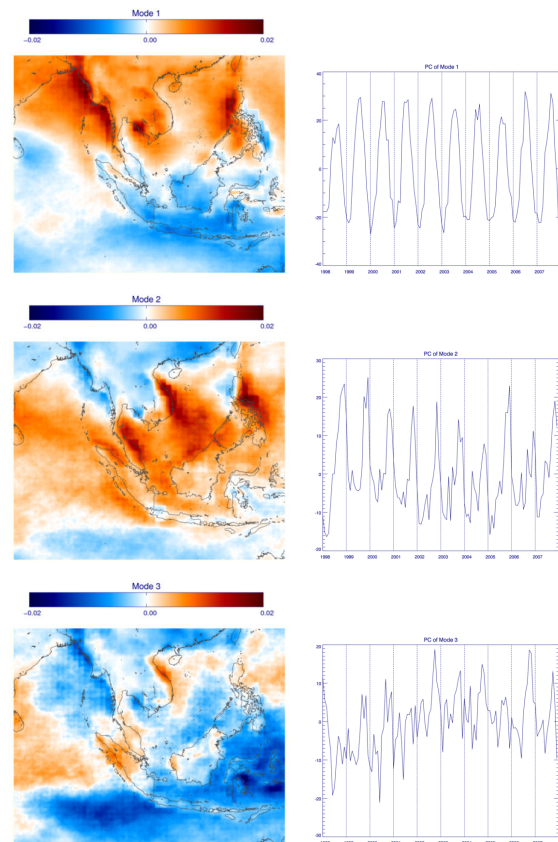
Fig. 10. The first three EOF modes of precipitation rate (left column, from the top) EOF1, EOF2 and EOF3. The corresponding temporal coefficients are shown on the right column.

The second mode EOF2 of the precipitation rate also shows a strong seasonal variation with two dominant periodic components of 12 and 6 months cycles. After the periodic components are subtracted away, the de-trend EOF2 temporal coefficient shows a correlation with the Ocean Nino Index (R^2=0.47). A similar analysis is performed on EOF3 and the EOF3 temporal anomaly exhibits a weaker correlation with the Ocean Nino Index ($R^2 = 0.38$).

5. CONCLUSION

In this study, time series analysis with linear regression and Fourier analysis have been applied to satellite records of environmental parameters relevant to climate change for the Southeast Asian region. Visualization of the increasing or decreasing trend in the parameters at different locations can be achieved from the maps of the regression slopes. EOF analysis relates the temporal variations to several forcing mechanisms.

SST and SLA were found to have increasing trends over the past one to two decades, consistent with the observations of global warming. The SST slope is about 0.2 degC per decade but the rate is higher near the southern coast of China. This higher warming trend may have implications on the occurrence and magnitude of tropical typhoon in this area. The AOT generally has near-zero slope but several areas with increasing AOT were observed where land clearing and biomass burning activities were common. The vegetation index generally shows a decreasing trend, possibly resulting from anthropogenic activities. EOF analysis reveals influence of El-Nino on SLA and precipitation rate. The results indicate usefulness of using satellite records of environmental parameters in climate change studies.

REFERENCES

Bjornsseon, H. and S. A. Venegas, " A manual for EOF and SVD analyses of climate data," McGill University CCGCR Report No. 97-1, Montréal, Québec, 52pp., 1997.

Huete, A, Justice, C and Van Leeuwen, W (1999): MODIS Vegetation Index (MOD 13) Algorithm Theoretical Basis Document. Available online at: http://modis.gsfc.nasa.gov/data/atbd/atbd_mod13.pdf

Huete, A, Didan, K, Miura, T, Rodriguez, E, Gao, X and Ferreira, L (2002): Overview of the radiometric and biophysical performance of the MODIS vegetation indices, Remote Sensing of Environment 83, 195-213.

Huffman, G. et al. (2007): "The TRMM multisatellite precipitation analysis (TMPA): Quasi-global, multiyear, combined-sensor precipitation estimates at fine scales," Journal of Hydrometeorology, vol. 8, Feb. 2007, pp. 38-55.

Kilpatrick., KA, Podesta., GP, and Evans., R. (2001): Overview of the NOAA/NASA advanced very high resolution radiometer Pathfinder algorithm for sea surface temperature and associated matchup dataset. J. Geophys. Res. 106(C5), 9179-9197.

King, M. et al. (2003), "Cloud and aerosol properties, precipitable water, and profiles of temperature and water vapor from MODIS," IEEE Transactions on Geoscience and Remote Sensing, vol. 41, Feb. 2003, pp. 442-458.

Leuliette, E.W., R.S. Nerem, and G.T. Mitchum, (2004): "Calibration of TOPEX/Poseidon and Jason Altimeter Data to Construct a Continuous Record of Mean Sea Level Change," Marine Geodesy, vol. 27, p. 79.

Lorenz, E. N., "Empirical orthogonal functions and statistical weather prediction," Sci. Rep. No. 1, Statistical Forecasting Project, MIT, Cambridge, MA, 48pp., 1956.